International Journal of Microwave and Wireless Technologies

cambridge.org/mrf

Compact ultra-wideband rectifier for environmental energy harvesting based on coupled structure

Dejin Zhu[1], Haoming He[1], Zhongqi He[1], Chongwei Liao[1] and Changjun Liu[2]

[1]Sichuan University, China and [2]School of Electronics and Information Engineering, Sichuan University, China

Research Paper

Cite this article: Zhu D, He H, He Z, Liao C, Liu C (2026) Compact ultra-wideband rectifier for environmental energy harvesting based on coupled structure. *International Journal of Microwave and Wireless Technologies*, 1–9. https://doi.org/10.1017/S1759078726103663

Received: 30 December 2025 UTC
Revised: 6 July 2026 UTC
Accepted: 9 July 2026 UTC

Keywords:
band-stop; energy harvesting; impedance matching; rectifier; ultra-wideband

Corresponding author: Changjun Liu;
Email: cjliu@ieee.org

Abstract

This paper presents a compact, ultra-wideband, and high-efficiency rectifier designed for microwave power transmission and energy harvesting applications. The proposed architecture integrates a series-coupled matching network with cascading band-stop structures, enabling both impedance transformation and harmonic control within a compact footprint. Two highly compact rectifiers are designed, fabricated, and measured to verify the proposed method. A broadband rectifier, operating between 1.8 and 3.0 GHz with a relative bandwidth of 50%, achieves above 70% rectification efficiency and a peak efficiency of 79%. The other wideband operation mechanism is analytically investigated: the band-stop network reshapes the diode's impedance profile by tuning its low- and high-frequency components into a conjugate relationship, while the coupled matching structure transforms the resulting impedance to match the system impedance, thereby realizing ultra-wideband matching. The fabricated rectifier achieves a measured efficiency exceeding 40% across a wide frequency range of 1.1–3.9 GHz, corresponding to a 112% relative bandwidth at a low input power level of 0 dBm. In addition to its wideband and efficient performance, the rectifier features a highly compact form factor of only $18 \times 24.8\ mm^2$.

Introduction

As an emerging wireless power transmission technology, microwave power transmission (MPT) and energy harvesting (EH) have attracted significant research attention due to their numerous advantages [1, 2]. These technologies offer a promising solution to the critical limitation of battery lifespan in wireless sensor networks (WSNs) [3, 4], thereby significantly improving power availability and enabling the broader deployment of WSNs across various application scenarios [5–7].

Within MPT and EH systems, two persistent challenges are maximizing the capture of incident electromagnetic energy and improving the radio frequency to direct current (RF-to-DC) conversion efficiency [8, 9]. A significant challenge in achieving high-efficiency wideband rectification is the nonlinear and frequency-dependent input impedance of the rectifying diode. This nonlinearity complicates the impedance matching process across a broad frequency range. To address this challenge, non-uniform transmission lines have been effectively employed to realize broadband impedance matching, enabling rectifiers to maintain high conversion efficiency over extended bandwidths [10, 11]. Additionally, the integration of harmonic termination techniques has been shown to improve bandwidth without increasing circuit dimensions [12, 13]. In terms of novel impedance compression techniques, the primary method to achieve small size and high efficiency is to compress the variation range of the rectifier's input impedance [14, 15]. To further enhance rectifier performance, several advanced strategies have been investigated. These include frequency-selective multi-branch architectures [16–18], complementary resonant structures for dynamic frequency-dependent switching [19], simplified real-frequency design techniques [20], and complex impedance-matching networks tailored for broadband operation [21, 22]. These approaches have contributed to the continued advancement of high-efficiency, wideband rectifier designs for next-generation wireless power systems.

An earlier version of this paper was presented at EuMW 2025 and was published in its Proceedings [23]. Compared with our previous work [24], which primarily focuses on efficiency enhancement, this paper analyzes the matching mechanism of the structure and, based on its operating characteristics, identifies the most suitable broadband matching impedance conditions for ultra-wideband rectifier applications. Two different rectifier prototypes were fabricated and experimentally validated to demonstrate the effectiveness of the proposed matching impedance approach over an ultra-wide bandwidth. This work places greater emphasis on the impedance-matching capability of the matching network over an ultra-wide frequency range. By properly selecting the impedance space, the operating bandwidth is significantly extended.

© The Author(s), 2026. Published by Cambridge University Press in association with The European Microwave Association.

Downloaded from https://www.cambridge.org/core. UNIVERSIDAD AUTONOMA METROPOLITANA, on 17 Nov 2026 at 19:08:23, subject to the Cambridge Core terms of use, available at https://www.cambridge.org/core/terms. https://doi.org/10.1017/S1759078726103663

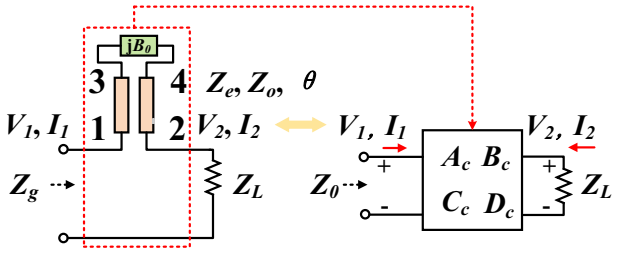


Figure 1. The proposed coupled matching structure and its equivalent two-port network.

Principle and design method

Analysis of the coupled matching structure

The schematic of the proposed coupled matching structure (CMS) is illustrated in Figure 1. The coupled transmission line has an electrical length of θ, with even- and odd-mode characteristic impedances denoted as Z_e and Z_o, respectively. A susceptive element with susceptance B_0 is connected between ports 3 and 4 of the coupled lines. The two-port network formed between ports 1 and 2 can be characterized using an ABCD matrix, which relates the source impedance Z_g to the load impedance Z_L. To facilitate theoretical analysis, the network is decomposed into even- and odd-mode excitation cases. The corresponding ABCD matrices for the even and odd modes are derived and denoted as [25]:

$$\begin{bmatrix} A_e & B_e \\ C_e & D_e \end{bmatrix} = \begin{bmatrix} \cos\theta & jZ_e \sin\theta \\ j\sin\theta/Z_e & \cos\theta \end{bmatrix} \tag{1}$$

$$\begin{bmatrix} A_o & B_o \\ C_o & D_o \end{bmatrix} = \begin{bmatrix} \cos\theta - 2B_0 Z_o \sin\theta & jZ_o \sin\theta \\ j(\sin\theta/Z_o + 2B_0 \cos\theta) & \cos\theta \end{bmatrix} \tag{2}$$

The two-port coupled-line network matrix is formulated as

$$\begin{bmatrix} A_c & B_c \\ C_c & D_c \end{bmatrix} = \begin{bmatrix} \frac{A_eC_o+A_oC_e}{A_eC_o-A_oC_e} & \frac{2A_eA_o}{A_eC_o-A_oC_e} \\ \frac{2C_eC_o}{A_eC_o-A_oC_e} & \frac{A_eC_o+A_oC_e}{A_eC_o-A_oC_e} \end{bmatrix} \tag{3}$$

By analyzing the ABCD matrix, we obtain the voltage reflection coefficient as

$$S_{11} = \frac{A_cZ_L + B_c - C_cZ_gZ_L - D_cZ_g}{A_cZ_L + B_c + C_cZ_gZ_L + D_cZ_g} \tag{4}$$

where $Z_L = R_L + jX_L$ is the load impedance, and R_L is greater than zero.

As an ideal impedance match, the condition $S_{11} = 0$. Equation (4) is simplified as

$$Z_e = \left(M_1 + \sqrt{M_1^2 + M_2}\right)\tan\theta \tag{5}$$

$$B_0 = \frac{M_2\tan^2\theta + Z_eZ_o}{2(Z_eZ_o - M_2)Z_o\tan\theta} \tag{6}$$

where $Z_g = R_S$, $R_L \neq R_S$ and

$$M_1 = \frac{R_SX_L}{R_L - R_S} \tag{7}$$

$$M_2 = \frac{R_SX_L^{\,2}}{R_L - R_S} + R_SR_L \tag{8}$$

Equations (5) to (8) indicate that the odd-mode impedance Z_o and θ are two independent design variables, unaffected by the load impedance Z_L or the source impedance R_s. This decoupling allows these parameters to be freely tuned, offering significant flexibility in the design of CMS for broadband rectifier applications. When the load impedance is symmetrically distributed along the real axis on the Smith chart, i.e., the load impedance Z_L at the center frequency f_0 is set to $Z_L = R_L$, and the load impedance at the start frequency f_1 and the stop frequency f_2 are $Z_{f1} = R_L - jX_{L1}$ and $Z_{f2} = R_L + jX_{L1}$, respectively. By solving the equation for Z_o and θ, CMS can successfully match the impedance at f_0, f_1, and f_2. At this point, the impedance across the entire frequency band is also matched to the microwave source impedance.

Based on this theoretical framework, the CMS can effectively transform arbitrary complex load impedances into the desired source impedance, enabling wideband impedance matching.

Design of the rectifier

Figure 2 illustrates the schematic of the proposed wideband rectifier. Part A is a band-stop structure formed by a series $\lambda_g/8$ short-ended transmission line, while Part B represents the CMS.

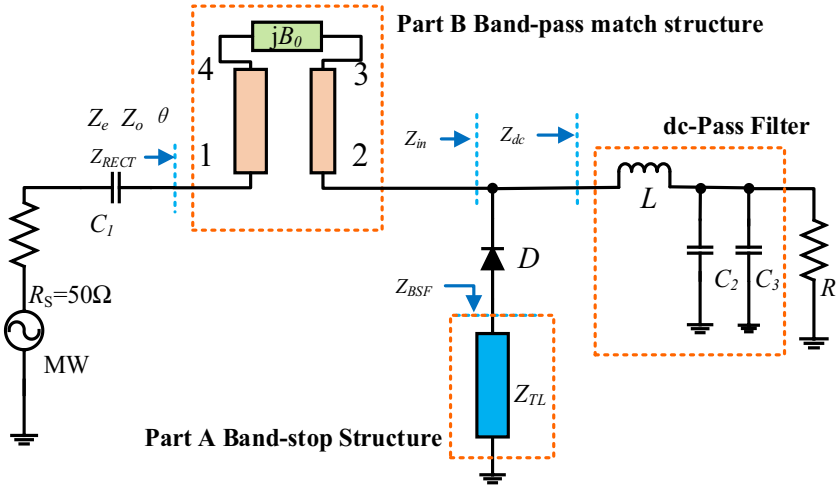


Figure 2. Proposed wideband rectifier I with the CMS.

Downloaded from https://www.cambridge.org/core. UNIVERSIDAD AUTONOMA METROPOLITANA, on 17 Nov 2026 at 19:08:23, subject to the Cambridge Core terms of use, available at https://www.cambridge.org/core/terms. https://doi.org/10.1017/S1759078726103663

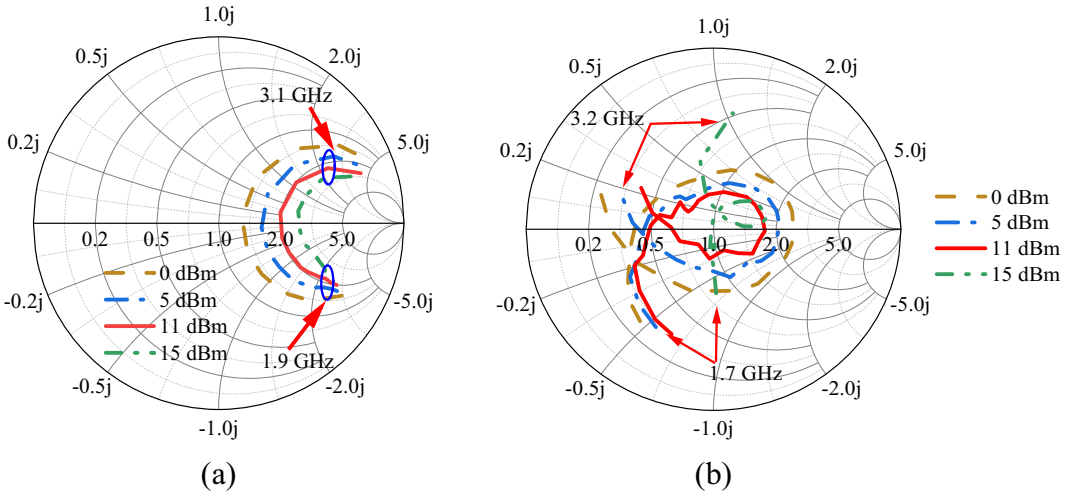


Figure 3. Zin over 1.9–3.1 GHz at various input power levels. (b) ZRECT over 1.7–3.2 GHz at different input power levels.

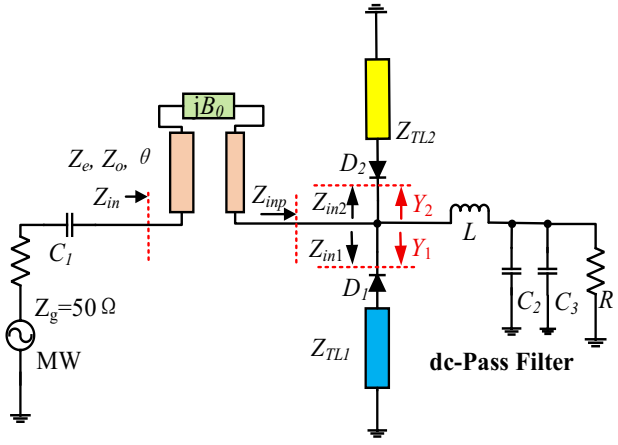


Figure 4. Schematic diagram of an ultra-wideband rectifier.

The input impedance of the $\lambda_g/8$ short-ended transmission line is

$$Z_{\mathrm{BSF}} = jZ_{\mathrm{TL}} \tan\left(\frac{\pi}{4}\frac{f}{f_0}\right) = \begin{cases} jZ_{\mathrm{TL}} \tan\left(\frac{\pi}{4}\frac{f}{f_0}\right) & 0 < f < f_0 \\ jZ_{\mathrm{TL}} & f = f_0 \\ jZ_{\mathrm{TL}} \tan\left(\frac{\pi}{4}\frac{f}{f_0}\right) & f_0 < f < 2f_0 \\ \infty & f = 2f_0 \end{cases} \tag{9}$$

where Z_{TL} is the characteristic impedance of the transmission line.

The impedance Z_{BSF} is inductive at f_0, compensating for the diode's capacitive reactance, i.e., $\mathrm{Im}(Z_D) = -Z_{\mathrm{TL}}$. It facilitates impedance matching at f_0. Z_{BSF} is infinite at $2f_0$, which helps to recycle the second harmonic at $2f_0$ during rectification. Thus, the rectification efficiency is improved.

Z_{dc} is the input impedance of the dc-pass filter, which provides an open circuit for all RF signals in the operating band. Z_{in} is equal to the parallel of the diode branch and the dc-filter. Thus, Z_{dc} is neglected. In this case, Z_{in} becomes the equivalent load to the CMS, i.e., $Z_L = Z_{in}$.

Z_{in} becomes the impedance of the diode in series with the band-stop structure as

$$Z_{in} = Z_D + Z_{\mathrm{BSF}} \tag{10}$$

Thus, Z_{in} is capacitive when $f < f_0$ and inductive when $f_0 < f < 2f_0$ from Equation (9).

We choose 2.45 GHz as the center frequency f_0 in the wideband rectifier design. Due to the analysis of the band-stop structure, Z_{in} is approximately located along a constant resistance circle on the Smith chart in the operating frequency band, as shown in Figure 3a. The band-stop structure compensates for the diode impedance at f_0 to become a resistance located at the real axis. Z_{in} is above the real axis when $f_0 < f < 2f_0$ and below the real axis when $f < f_0$, distributed almost conjugately around the real axis in the Smith chart.

Therefore, the imaginary part of the impedance of the diode series with the band-stop structure at an input power level is

$$Im\left(Z_{in}\right)|_{f=f_0} = Im\left(Z_D + Z_{\mathrm{BSF}}\right)|_{f=f_0} \tag{11}$$

The load impedance Z_L at the center frequency f_0 is set to $Z_L = R_L$. Then, the load impedance at the start frequency f_1 and the stop frequency f_2 is $Z_{f1} = R_L - jX_{L1}$ and $Z_{f2} = R_L + jX_{L1}$, respectively.

Based on the analysis of the band-stop structure, the input impedance Z_{in} is approximately distributed along a constant-resistance circle on the Smith chart over the operating frequency band, as shown in Figure 3a. Accordingly, the load impedance is defined as $Z_L = R_L$, while the input impedances at the center frequency f_0, start frequency f_1, and stop frequency f_2 are expressed as $Z_{f1} = R_L - jX_{L1}$ and $Z_{f2} = R_L + jX_{L1}$, respectively.

For optimal rectifier operation, the input impedance must be matched to the system characteristic impedance, i.e., $Z_0 = 50\ \Omega$. Consequently, the source impedance is set to $Z_0 = R_s = 50\ \Omega$. Substituting these conditions into Equations (8) and (9) yields Equations (13) and (14).

$$M_1 = \frac{Z_0 X_{\mathrm{L}}}{R_{\mathrm{L}} - Z_0} \tag{12}$$

$$M_2 = \frac{Z_0 X_{\mathrm{L}}^{\ 2}}{R_{\mathrm{L}} - Z_0} + Z_0 R_{\mathrm{L}} \tag{13}$$

Downloaded from https://www.cambridge.org/core. UNIVERSIDAD AUTONOMA METROPOLITANA, on 17 Nov 2026 at 19:08:23, subject to the Cambridge Core terms of use, available at https://www.cambridge.org/core/terms. https://doi.org/10.1017/S1759078726103663

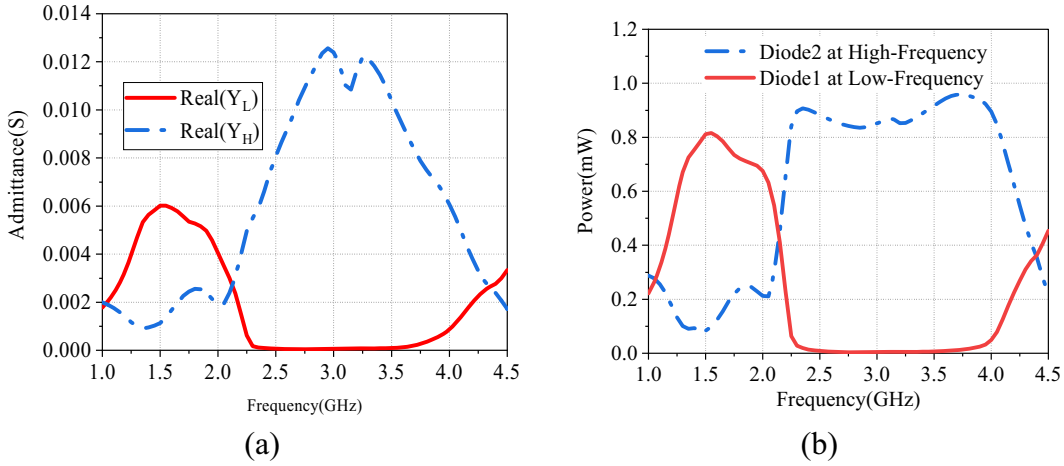


Figure 5. (a) The admittance of the two branches of the rectifier. (b) Simulation power of diodes 1 and 2 versus frequency.

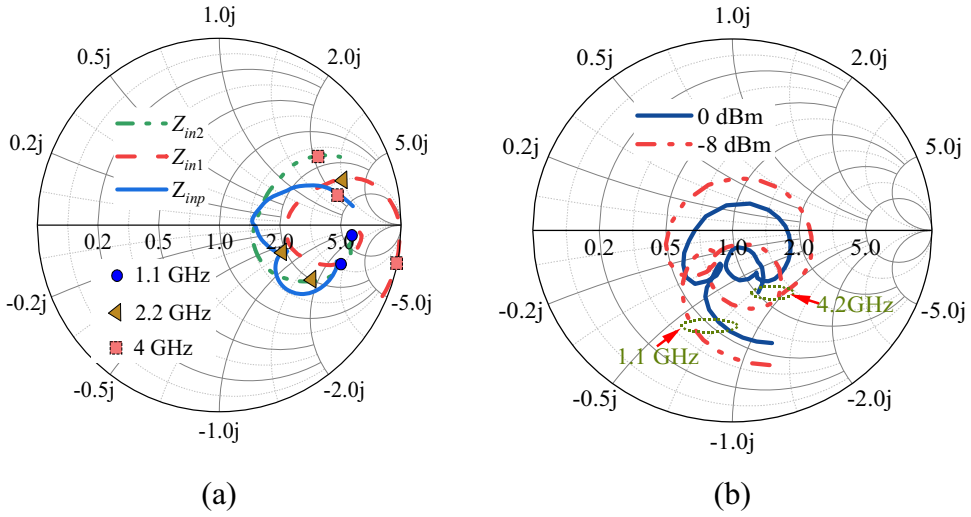


Figure 6. (a) Impedance transformation over 1–4.2 GHz of ultra-wideband rectifier at 0 dBm. (b) Z_{in} over 1–4.2 GHz of ultra-wideband rectifier.

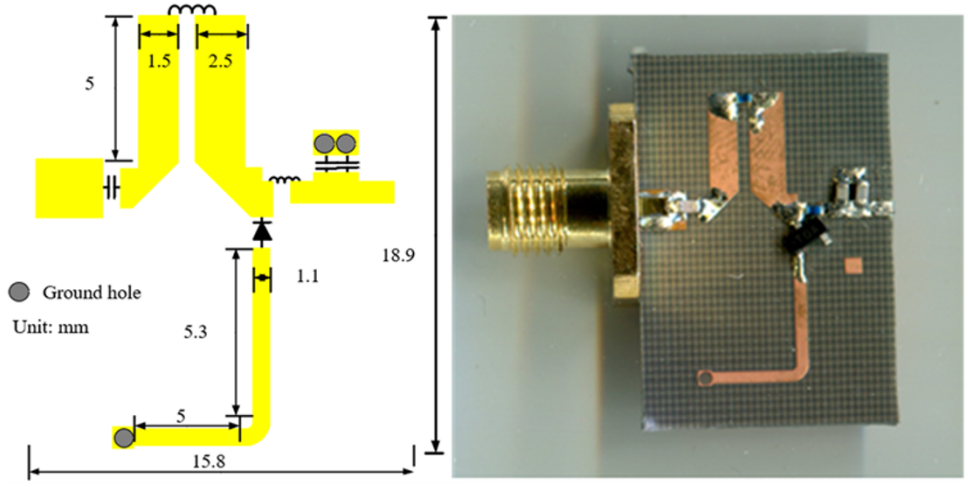


Figure 7. Layout and photograph of the rectifier with parameter details.

Downloaded from https://www.cambridge.org/core. UNIVERSIDAD AUTONOMA METROPOLITANA, on 17 Nov 2026 at 19:08:23, subject to the Cambridge Core terms of use, available at https://www.cambridge.org/core/terms. https://doi.org/10.1017/S1759078726103663

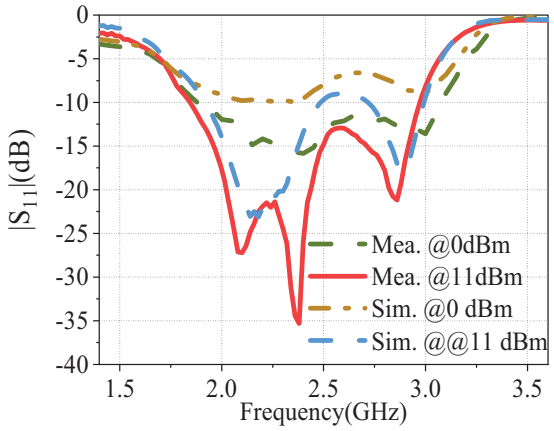


Figure 8. S-parameter curves of the broadband rectifier.

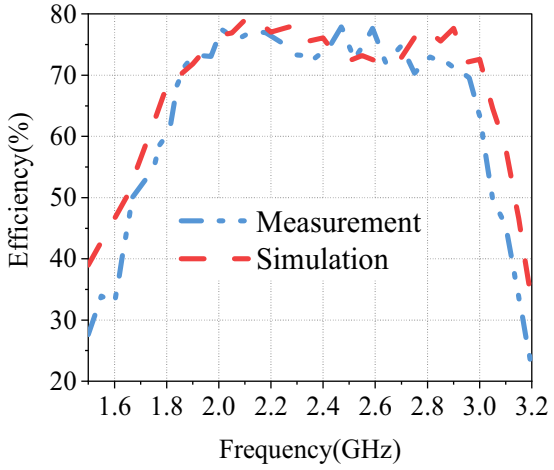


Figure 9. Efficiency curves of broadband rectifier I at 11 dBm.

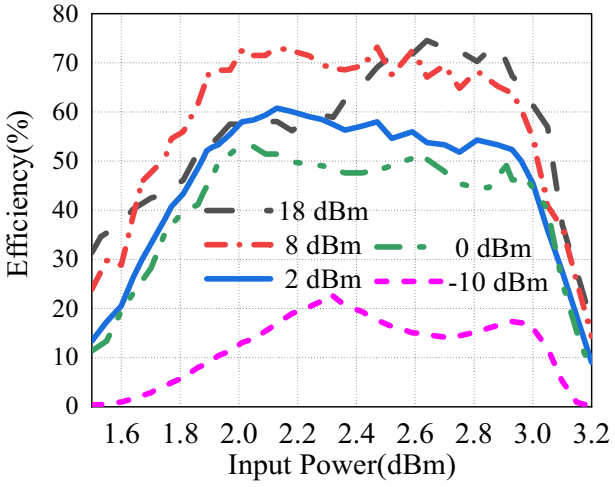


Figure 10. Efficiency curves of broadband rectifier I at different powers.

$$Z_e = \left(-M_1(f_1) + \sqrt{M_1^2(f_1) + M_2(f_1)}\right) \tan\left(\theta_0 \frac{f_1}{f_0}\right) = \left(M_1(f_2) + \sqrt{M_1^2(f_2) + M_2(f_2)}\right) \tan\left(\theta_0 \frac{f_2}{f_0}\right) \quad (14)$$

Since the even-mode impedance Z_e exhibits minimal variation with frequency, it is possible to establish equations to determine the electrical length θ and achieve impedance matching at both f_1 and f_2. Notably, the load impedances at f_1 and f_2 are approximately complex conjugates, leading to identical values of M_2, i.e., $M_2(f_1) = M_2(f_2)$, while M_1 exhibits opposite signs, such that $M_1(f_1) = -M_1(f_2)$. As shown in Equation (12), the electrical length at the center frequency, denoted as θ_0, is selected as the electrical length of the CMS. Through this approach, a value of θ_0 is derived that enables conjugate impedance matching simultaneously at the start and stop frequencies.

Further analysis reveals that the susceptive element in the CMS is an inductor L_0. For a given inductance value, the susceptance $B_0(f_0)$ varies with frequency, where $B_0(f_0)$ and $B_0(f_2)$ correspond to the susceptance at the center frequency $B_0(f_0)$ and stop frequency f_2, respectively. As shown in Equations (13) and (14), by exploiting the frequency-dependent behavior of the inductor L_0 to satisfy both $B_0(f_0)$ and $B_0(f_2)$, the characteristic impedance Z_o can be derived, thereby enabling simultaneous impedance matching at f_0 and f_2. As a result, the CMS achieves effective impedance matching at all three critical frequency points: f_0, f_1, and f_2.

$$B_0(f)|f_0 = \frac{1}{2\pi j f_0 L_0} = \frac{M_2(f_0)\tan^2(\theta_0) + Z_e Z_o}{2\left(Z_e Z_o - M_2(f_0)\right) Z_o \tan(\theta_0)} \quad (15)$$

$$B_0(f)|_{f_2} = \frac{1}{2\pi j f_2 L_0} = \frac{M_2(f_2)\tan^2\left(\theta_0 \frac{f_2}{f_0}\right) + Z_e Z_o}{2\left(Z_e Z_o - M_2(f_2)\right) Z_o \tan\left(\theta_0 \frac{f_2}{f_0}\right)} \quad (16)$$

Although achieving perfect impedance matching across the entire operating bandwidth is inherently challenging, matching at the three representative frequencies – start f_1, center f_0, and stop f_2 – provides a practical and effective design strategy. All parameters were subsequently fine-tuned using full-wave and circuit-level simulations to further optimize performance. As shown in Figure 3b, the rectifier input impedance remains close to 50 Ω across the operating band, confirming the effectiveness of the proposed impedance-matching approach.

Design of the ultra-wideband rectifier

To further validate the proposed wideband rectifier approach, an ultra-wideband low-power rectifier is designed, as illustrated in Figure 4. This rectifier features a dual-diode configuration, where D_1 and D_2 are connected in parallel, each in series with a dedicated band-stop structure. D_1 is optimized to operate at lower frequencies, while D_2 is tailored for higher frequencies, allowing for impedance compression across distinct frequency ranges.

The power flowing into the different diodes satisfies

$$\frac{P_1}{P_2} = \frac{\text{real}(Y_1)}{\text{real}(Y_2)} \quad (17)$$

P_1 and P_2 are the energies flowing into the two diodes, and Y_1 and Y_2 are the corresponding admittances. It can reduce the interference caused by the two diodes by setting the length of the microstrip line. Two short-circuited transmission lines are employed for band-selective control: TL1, designed as $\lambda_g/8$ at low frequencies, governs the low-frequency operation, and TL2, also $\lambda_g/8$ but at higher frequencies, enhances performance in the high-frequency range. An effective setting is that the lengths of the two microstrip lines satisfy $\theta_L \approx 2\theta_H$, and the impedance is infinite

Downloaded from https://www.cambridge.org/core. UNIVERSIDAD AUTONOMA METROPOLITANA, on 17 Nov 2026 at 19:08:23, subject to the Cambridge Core terms of use, available at https://www.cambridge.org/core/terms. https://doi.org/10.1017/S1759078726103663

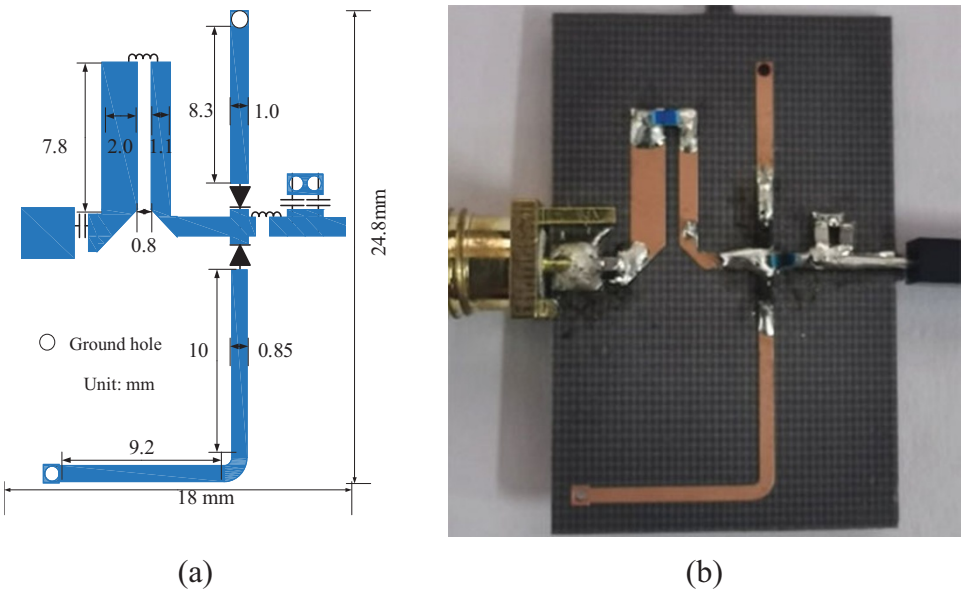


Figure 11. (a) Layout of the proposed ultra-wideband rectifier. (b) Photograph of the fabricated ultra-wideband rectifier.

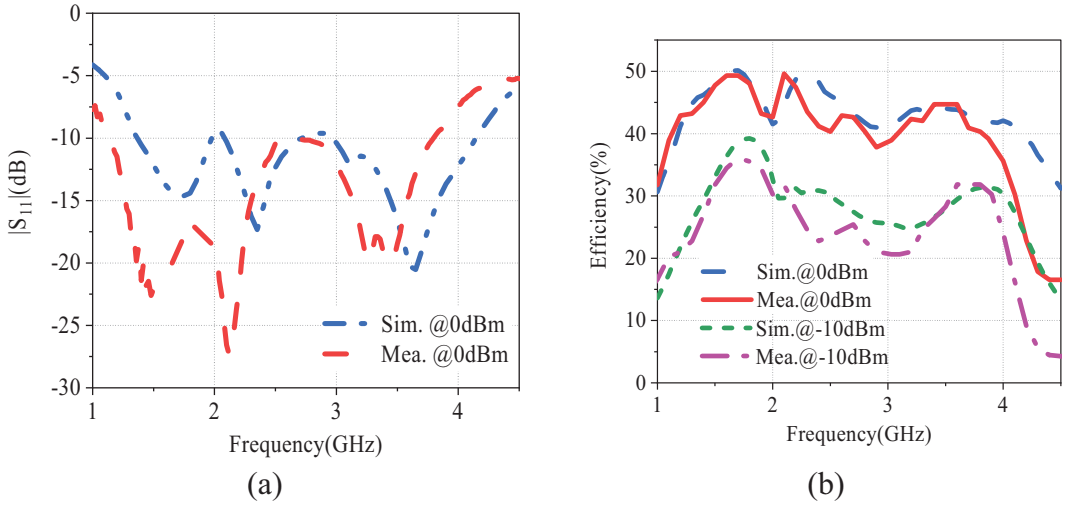


Figure 12. (a) The reflection coefficient |S11| of the ultra-wideband rectifier at 0 dBm. (b) RF-dc conversion efficiency versus frequency simulated and measured at 0 dBm and −8 dBm of the rectifier.

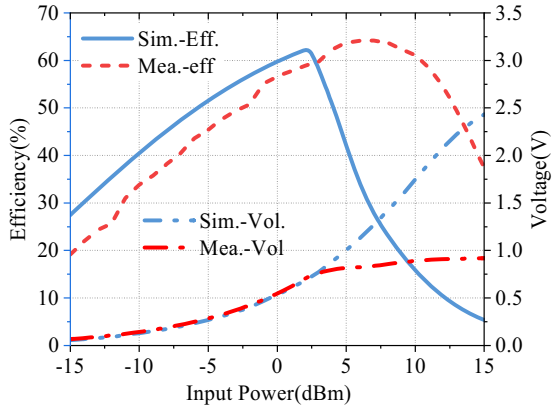


Figure 13. Conversion efficiency and output dc voltage at 1.7 GHz.

when the frequency is increased to an octave of the low frequency; basically, there is no power flowing into the low-frequency diode.

The admittance of the two branches of the rectifier at different frequencies is shown in Figure 5a. Figure 5b shows the distribution of RF power between the two diodes across different frequencies. Under a 0 dBm (1 mW) input, the majority of the RF power is directed to D_1 within the 1.1–2.2 GHz range. As the frequency increases, D_2 gradually dominates, receiving more than 80% of the power in the 2.2–4.1 GHz band, while the power loss in D_1 becomes negligible.

The input impedance responses of the diodes under 0 dBm excitation are presented in Figure 6a. The impedance trajectories – denoted as Z_{in1}, Z_{in2}, and Z_{inp} are approximately symmetric to the real axis across their corresponding bands: 1.1–2.2 GHz for D_1, 2.2–4.0 GHz for D_2, and 1.1–4.0 GHz for the total network. A conjugate impedance pattern in which all three impedance curves approximately satisfy the matching requirements.

Downloaded from https://www.cambridge.org/core. UNIVERSIDAD AUTONOMA METROPOLITANA, on 17 Nov 2026 at 19:08:23, subject to the Cambridge Core terms of use, available at https://www.cambridge.org/core/terms. https://doi.org/10.1017/S1759078726103663

Table 1. Comparison between ultra-wide rectifiers

Ref	Diode	Input power (dBm)	Efficiency requirement	Band range (GHz)	Fraction bandwidth (%)	Size (mm^2)	Diode number
[18]	HSMS282B	8–25	50%	1.82–2.75	40.7	34 × 17	2
[10]	SMS7630	0	40%	0.43–0.95	75.36	190 × 30	2
[15]	HSMS2852	8	40%	1.4–2.6	80	33 × 36	4
[14]	HSMS2852	6.5	40%*	1.1–2.9	90	30 × 26	4
[17]	SMS7630	9	40%*	1.2–3.2	104	N. A	4
[19]	HSMS2850	6	50%	0.32–0.92	107.7	38 × 100	1
[21]	SMS7630	0	40%*	0.8–2.4	100	32 × 14	2
This work	SMS7630	0	40%	1.1–3.9	112	18 × 25	2

The three important frequencies of the rectifier were set to $f_0 = 2.2$ GHz, $f_1 = 1.1$ GHz, and $f_2 = 4$ GHz. The input impedances $Z_{in}(f_1)$ and $Z_{in}(f_2)$ were obtained and calculated in Equation (14), and θ_0 was obtained. Then, substituting $Z_{in}(f_0)$ into Equation (5) yields Z_e. Employing Equations (15) and (16) establishes $B_0(f_1)/B_0(f_2) = f_2/f_1$, and Z_o was determined. At last, B_0 is calculated. Figure 6b illustrates the input impedance Z_{IN} of the rectifier after applying the CMS. The results indicate excellent impedance matching across a wideband range of 1.3–4.1 GHz.

Implementation and measurements

Rectifier I

The layout and physical prototype of the broadband rectifier are shown in Figure 7 with an F4B-2 substrate (dielectric constant of 2.65 and loss tangent of 0.0012). The specific design parameters are detailed in Figure 7 as well, and the inductance of the susceptive element is 2.7 nH, and the diode is HSMS286.

The simulated and measured S-parameters are presented in Figure 8, showing good agreement between simulation and measurement. For input power levels of 0 dBm and 11 dBm, the measured $|S_{11}|$ remains below −10 dB over the frequency range of 1.8–3.0 GHz, indicating effective wideband impedance matching.

The rectifier power conversion efficiency was subsequently evaluated. Figure 9 compares the simulated and measured rectification efficiencies at an input power of 11 dBm with a 500 Ω DC load, demonstrating close agreement. The measured efficiency exceeds 70% across 1.8–3.0 GHz, corresponding to a fractional bandwidth of 50%. As shown in Figure 10, the efficiency remains above 50% from 1.88 to 2.98 GHz as the input power varies from 2 to 18 dBm.

Ultra-wideband rectifier

The layout of the design and the photograph of the rectifier are shown in Figure 11a and 11b, respectively. It uses two SMS7630 diodes, and its total size is 18 × 24.8 mm.

The measured reflection coefficient $|S_{11}|$ at an input power of 11 dBm is presented in Figure 12a. At an input of 0 dBm, the ultra-wideband rectifier exhibits excellent impedance matching, with $|S_{11}|$ remaining below −10 dB over the 1.1–3.9 GHz frequency range, thereby confirming its wideband matching performance. The RF-to-DC conversion efficiency versus frequency at input power levels of 0 dBm and −8 dBm is shown in Figure 12b, measured with a 200 Ω load. At 0 dBm, the rectifier achieves over 40% efficiency across the 1.1–3.9 GHz band, corresponding to a fractional bandwidth of 112%. Even at a reduced input power of −8 dBm, the efficiency remains above 20% over the extended frequency range of 1.05–4.05 GHz, highlighting the rectifier's robust low-power performance. Figure 13 illustrates the variation in efficiency as a function of input power. The highest recorded efficiency is 64.2% at 1.7 GHz.

Table 1 compares the performance with previous publications for ultra-wide bands. The fractional bandwidths of the proposed rectifiers are in the leading position, while their physical dimensions are much less than those of rectifiers of similar types. Rectifiers designed with CMS ensure high rectification efficiency and wide operating bandwidth at low and medium power levels while effectively reducing the physical size of the rectifier circuit.

Conclusion

This paper proposes a novel design for wideband rectifiers. A band-stop structure is applied to tune the diode impedance and enhance the conversion efficiency. A coupled matching structure successfully matches it to the system impedance within a wide bandwidth. We explored the mechanism and presented the design methods.

Two wideband rectifiers were designed, fabricated, and measured to verify the proposed design method. The operating bandwidths of the two rectifiers are from 1.83 to 2.95 GHz and from 1.1 to 3.9 GHz, respectively. They have very compact physical dimensions as well. The design methodology helps facilitate the design of wide-band compact rectifiers and makes them easier to integrate into antennas. They have a bright future in the applications of wireless power transmission and EH systems.

Acknowledgements. This work was supported in part by the Natural Science Foundation of China (NSFC) under Grants U22A2015 and 62401382 and JCKY.

Author contributions. D.Z. and C.L. derived the theory; H.H. and Z.H. performed the simulations. All authors contributed equally to analyzing data and reaching conclusions and in writing the paper.

Competing interest. The authors declare none.

References

1. **Wu Y and Liu G** (2025) Analysis of continuous mode class-B/J efficiency model for broadband rectifier. *International Journal of Microwave and Wireless Technologies* 1–8. https://doi.org/10.1017/S1759078725102456
2. **Du C-H, Cheng F, Wu L and Gu C** (2024) Efficient broad dual-band voltage doubler rectifier with multi-section line impedance matching network. *International Journal of Microwave and Wireless Technologies* **16**(7), 1133–1137. https://doi.org/10.1017/S1759078724001363

Downloaded from https://www.cambridge.org/core. UNIVERSIDAD AUTONOMA METROPOLITANA, on 17 Nov 2026 at 19:08:23, subject to the Cambridge Core terms of use, available at https://www.cambridge.org/core/terms. https://doi.org/10.1017/S1759078726103663

3. **He H, Liao C, He Z, Yan L and Liu C**. (2025) An arbitrary-frequency dual-band high-efficiency rectifier employing a novel frequency-selective power allocation network. *IEEE Transactions on Power Electronics* **40**(7), 8939–8943. https://doi.org/10.1109/TPEL.2025.3548282.
4. **Shinohara N** (2021) Trends in wireless power transfer: WPT technology for energy harvesting, millimeter-wave/THz rectennas, MIMO-WPT, and advances in near-field WPT applications. *IEEE Microwave Magazine* **22**, 46–59. https://doi.org/10.1109/MMM.2020.3027935
5. **He H, Zhou Y, He Z, Feng Y and Liu C** (2025) High-efficiency octave bandwidth rectifier for electromagnetic energy harvesting. *IEEE Microwave and Wireless Components Letters* **35**, 549–552. https://doi.org/10.1109/LMWT.2024.3510153
6. **Lin H, Chen X, He Z, Xiao Y, Che W and Liu C** (2021) Wide input power range X-band rectifier with dynamic capacitive self-compensation. *IEEE Microwave and Wireless Components Letters* **31**, 525–528. https://doi.org/10.1109/LMWC.2021.3067068
7. **Paolini G, Battistini G, Di Renzo ADF, Fazzini E, Tiberi T, Trovarello S, Masotti D and Costanzo A** (2024) On-demand beamforming and wide dynamic power range for WPT and EH applications. *International Journal of Microwave and Wireless Technologies* **16**(6), 903–918. https://doi.org/10.1017/S1759078724001065
8. **Liu C, Tan F, Zhang H and He Q** (2017) A novel single-diode microwave rectifier with a series band-stop structure. *IEEE Transactions on Microwave Theory and Techniques* **65**, 600–606. https://doi.org/10.1109/TMTT.2016.2626286
9. **He H, Liao C, He Z, Yan L and Liu C** (2025) High-efficiency ultrawideband microwave rectifier based on adaptive harmonic control. *IEEE Transactions on Microwave Theory and Techniques* **73**, 10017–10027. https://doi.org/10.1109/TMTT.2025.3624399
10. **Bolos F, Belo D and Georgiadis A**, "A UHF rectifier with one octave bandwidth based on a non-uniform transmission line," *2016 IEEE MTT-S International Microwave Symposium (IMS)*, San Francisco, CA, USA, 2016, pp. 1–3.
11. **Wu P et al** (2019) Compact high-efficiency wideband rectifier with multistage-transmission-line matching. *IEEE Transactions on Circuits and Systems II: Express Briefs* **66**(8), 1316–1320.
12. **He H, Lin H, Wu P, Li Q and Liu C** (2022) Compact high-efficiency broadband rectifier based on coupled transmission line. *IEEE Transactions on Circuits and Systems II: Express Briefs* **69**(11), 4404–4408. Nov.
13. **Bui GT, Nguyen D-A and Seo C** (2023) A highly efficient design of broadband rectifier with harmonic suppression transferring for energy harvesting and wireless power transfer. *IEEE Microwave and Wireless Components Letters* **33**, 1059–1062. https://doi.org/10.1109/LMWT.2023.3263523
14. **Bo SF, Ou J-H and Zhang XY** (2022) Ultrawideband rectifier with extended dynamic-power-range based on wideband impedance compression network. *IEEE Transactions on Microwave Theory and Techniques* **70**, 4026–4035. https://doi.org/10.1109/TMTT.2022.3179538
15. **Ming Wang P, Fei Bo S, Ou J-H and Yin Zhang X** (2025) High-efficiency wideband RF rectifier with enhanced dynamic power range based on impedance regulation network. *IEEE Microwave and Wireless Components Letters* **35**, 306–309. https://doi.org/10.1109/LMWT.2024.3523763
16. **Wu P, Huang SY, Zhou W and Liu C** (2018) One-octave bandwidth rectifier with a frequency selective diode array. *IEEE Microwave and Wireless Components Letters* **28**, 1008–1010. https://doi.org/10.1109/LMWC.2018.2869281
17. **Mansour M, Polozec XL and Kanaya H**. (2019) Enhanced broadband RF differential rectifier integrated with archimede and spiral antenna for wireless energy harvesting applications. *Sensors* **19**(655), 1–13. https://doi.org/10.3390/s19030655.
18. **Liu X, Ou J-H, Zhang D-W, Gui Z, Zhang B and Li Y-S** (2026) A miniaturized broadband rectifier with wide input power range based on adaptive input power distribution. *IEEE Microwave and Wireless Components Letters* **36**, 213–216. https://doi.org/10.1109/LMWT.2025.3624310
19. **Lu P, Song C and Huang KM** (2021) Ultra-wideband rectenna using complementary resonant structure for microwave power transmission and energy harvesting. *IEEE Transactions on Microwave Theory and Techniques* **69**, 3452–3462. https://doi.org/10.1109/TMTT.2021.3067902
20. **Lin YL, Zhang XY, Du Z-X and Lin QW** (2018) High-efficiency microwave rectifier with extended operating bandwidth. *IEEE Transactions on Circuits and Systems II: Express Briefs* **65**(7), 819–823. Jul.
21. **Liu W, Huang K, Wang T, Hou J and Zhang Z** (2022) A Compact High-Efficiency RF Rectifier with Widen Bandwidth. *IEEE Microwave and Wireless Components Letters* **32**, 84–87. https://doi.org/10.1109/LMWC.2021.3115106
22. **Cheng F, Du C-H, Wu L and Gu C** (2024) Compact and ultra-wideband high-efficiency rectifier using asymmetric coupled-line impedance transformer. *International Journal of Microwave and Wireless Technologies* **16**(6), 966–971. https://doi.org/10.1017/S1759078724000813
23. **He H, Song K, He Z, Yan L and Liu C**, "Small high-efficiency broadband rectifier based on compact coupled structure," 2025 55th European Microwave Conference (EuMC), Utrecht, Netherlands, 2025, pp. 318–321, https://doi.org/10.23919/EuMC65286.2025.11235269
24. **He H, Zhou Y, Ren P, Yan L, He Z and Liu C** (2026) A harmonic self-control network for compact high-efficiency rectifiers with extended bandwidth. *IEEE Microwave and Wireless Technology Letters* **36**(6), 1063–1066. https://doi.org/10.1109/LMWT.2026.3659794.
25. **Pozar DM** (2011) *Microwave Engineering*. Hoboken, NJ: John Wiley & sons.



Dejin Zhu received the M.S. degree in radio physics from Sichuan University, Chengdu, China, in 2006, where he is currently pursuing the Eng.D. degree in electronic information. His main research interests are the design and optimization of sensors and wireless power transmission.



Haoming He received the S. and M.S. degrees from Sichuan University, Chengdu, China, in 2020 and 2023, respectively, where he is currently pursuing the Ph.D. degree in Electronic Science and Technology. His current research interests include wireless power transmission and energy harvesting.



Zhongqi He received the M.S. degree and the Ph.D. degree in radio physics from Sichuan University, Chengdu, China, in 2018 and 2023, respectively. From 2021 to 2022, he was a visiting scholar at the University of Bologna, Italy. In 2023, he joined the College of Electronics and Information Engineering, Sichuan University, where he has been an associate research fellow since May 2025.He has authored more than 20 papers published in peer-reviewed journals and international conferences. His current research interests include wireless power transmission and energy harvesting.



Chongwei Liao received the B.S. degree in electronic information science and technology from Chengdu University of Information Technology, Sichuan, China, in 2017, and the M.S. degree in electromagnetic fields and microwave technology and the Eng.D. degree in electronic information from Sichuan University, Sichuan, China, in 2021 and 2025, respectively.His current research interests include industrial applications of microwave energy, microwave intelligent control, and microwave measurement.

Downloaded from https://www.cambridge.org/core. UNIVERSIDAD AUTONOMA METROPOLITANA, on 17 Nov 2026 at 19:08:23, subject to the Cambridge Core terms of use, available at https://www.cambridge.org/core/terms. https://doi.org/10.1017/S1759078726103663



Changjun Liu received the M.S. and Ph.D. degrees from Sichuan University, China, in 1997 and 2000, respectively. From 2000 to 2001, he was a post-doctoral researcher at Seoul National University, Korea. From 2006 to 2007, he was a visiting scholar at Ulm University, Germany. Since 1997, he has been with the Department of Radio-Electronics, Sichuan University, where he has been a professor since 2004. He has authored two books and more than 200 articles. His current research interests include microwave wireless power transmission and microwave power industrial applications. Dr. Liu was a recipient of the Outstanding Reviewer of the IEEE Transactions on Microwave Theory and Techniques from 2006 to 2010. He is a member of IEEE MTT-S TC 25 and serves as a topic editor of the IEEE Journal of Microwave. He also serves as the editor-in-chief of Microwave.

Downloaded from https://www.cambridge.org/core. UNIVERSIDAD AUTONOMA METROPOLITANA, on 17 Nov 2026 at 19:08:23, subject to the Cambridge Core terms of use, available at https://www.cambridge.org/core/terms. https://doi.org/10.1017/S1759078726103663